Modelling Pre and Post Acid Stimulation of Well T4, Mt. Apo Geothermal Field, Philippines

Mark Angelo O. Malibiran[1], Sadiq J. Zarrouk[2]*

[1]Energy Development Corporation, Pasig City, Philippines

[2] Department of Engineering Sciences, University of Auckland, Private Bag 92019, Auckland, New Zealand

malibiran.mo@energy.com.ph, *s.zarrouk@auckland.ac.nz

Keywords: *Reservoir modelling, acid stimulation, well test analysis,* Saphir™

ABSTRACT

The Mount Apo Geothermal Field is located on the northwestern flank of Mount Apo the Philippines' highest peak. Out of the 40 wells drilled in the field, 20 production and 8 injection wells are used to run the two 52 MWe plants commissioned in 1997 and 1999 respectively. During the cementing of the production casing of well T7, cement invaded the production zone of well T4 causing it to cease producing. Pressure transient data were collected and analyzed from injection/fall-off tests at different stages: post-drilling, after cement-damaged, after mechanical clearing and after acid stimulation. The preliminary analysis of the four sets of data is done using well test analysis and interpretation software (Saphir™). Three different numerical models were also developed to model the pressure transient for each test using: (a) a 3D model with a refined grid, (b) a radial model, and (c) a 3D model with a radial grid embedded into the injection block. For the radial-grid, three different types were further investigated: (a) homogeneous porous model, (b) fractured media model, and (c) a fractional dimension (fractal) model. The homogenous porous media model provided the best match to the pressure transient well test data.

1. INTRODUCTION

1.1 Mount Apo Geothermal Field

The Mount Apo Geothermal Field is located on the northwestern flank of Mount Apo volcano which, at 2954 m above sea level, is the Philippines' highest peak. The field is located in Kidapawan City, North Cotabato in the central part of the island of Mindanao, Philippines. It lies within the 701-hectares geothermal reservation area carved out from the 52,200 hectares of Mount Apo National Park. The geothermal field is geographically divided into three major sectors, namely, Matingao-Kullay, Marbel, and Sandawa (Figure 1).

There are 40 wells drilled in the field, 29 production wells and 11 wells for brine and condensate injection. Power generation in Mount Apo was developed in two stages. The first stage, the Mindanao 1 (M1GP) single flash 52 MWe Plant, was commissioned in March 1997 withten production wells supplying the plant. The second stage development commenced with the commissioning of the Mindanao 2 (M2GP) 52MWe double-flash turbine unit in June 1999. The steam supplied to this plant comes from eight production wells in the Sandawa sector, two wells in Marbel Corridor (Figure 1), and steam from the secondary flash of brine from the M1GP wells. Of the eight hot brine injection wells in the area, one infield injection well situated in Sandawa sector is dedicated for M2GP brine injection. The seven other injection wells are located in Matingao-Kullay area where five wells are used for M1GP hot brine injection and two wells are for cold condensate injection.

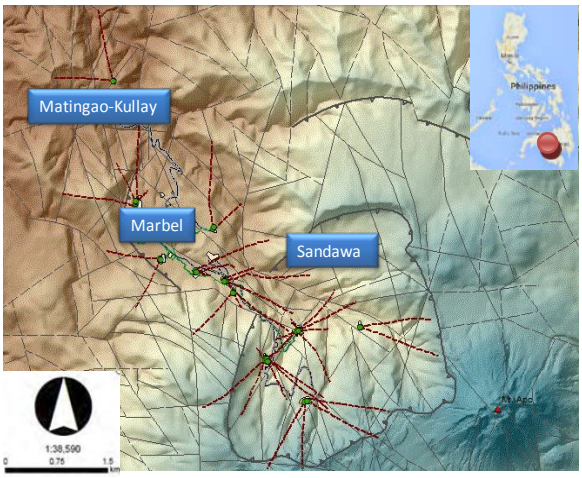

Figure 1: Location map of the Mount Apo Geothermal Project showing the well tracks, geologic faults and the main sectors (from Marasigan, 2014)

1.2 Well T4

Well T4 is the twenty-seventh production well drilled in the Mount Apo Geothermal Field located at site F, in Sandawa Sector. T4 was spudded on the 27th of December 1996 and took 29 days to attain the depth of 1066.62 mMD instead of the target depth of 1250 mMD. Well drilling was prematurely terminated due to recurring fills (sloughing formations) encountered at the bottom whereby drilling cannot advance any further. The rig was released on February 3, 1997. The well was designed with a four-string casing followed by a production liner configuration (Figure 2).

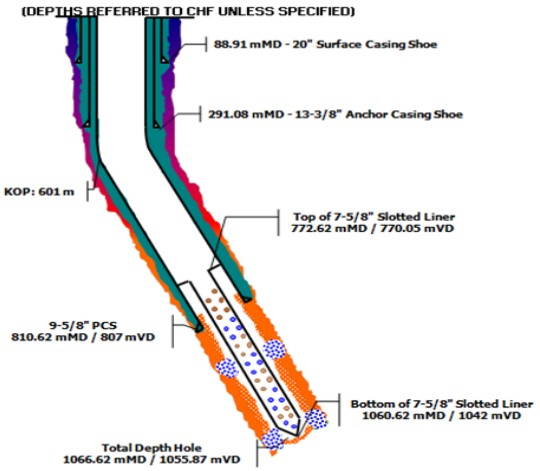

Figure 2: Well T4 casing profile

2. INTERFERENCE OF WELL T4 WITH WELL T7 DRILLING

On March 27, 2013, well T4 collapsed as a result of drilling interference with well T7, the seventh production well drilled in Site F. This was manifested during tripping at M2GP Power Plant where plant load was significantly reduced from 42.56 MWe net to 37.87 MWe. Figure 3 shows the plan view of T4 and T7 with the common structure TC fault.

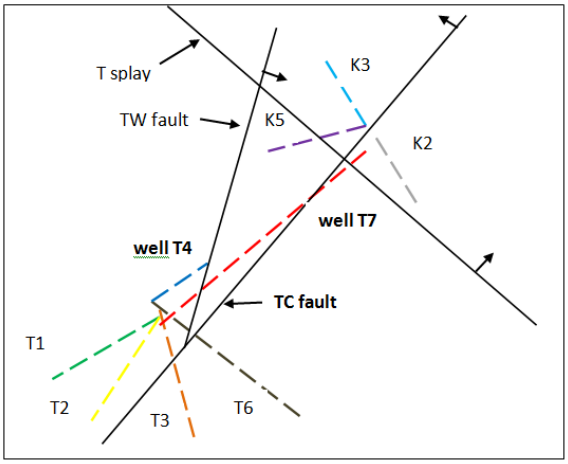

Figure 3: Plan views of wells T4 and T7 and the nearby faults

2.1 Cement Encroachment

Some ejecta were collected during attempted discharge of T4 on May 15, 2013 (Figure 4). A blockage survey was then conducted in well T4 on May 18, 2013 and tagged an obstruction at 818 mMD.

Figure 4: Ejecta collected during T4 attempted discharge

Tests showed that collected ejecta can be dissolved in hydrochloric acid solution, suggesting cement encroachment from well T7. Cement may have reached well T4 through TC fault during the cementing of the 9-5/8" production casing of well T7 on March 29, 2013. Downhole Viewer (DHV) survey on May 22, 2013 confirmed blockage at 810 mMD and some slots of the 7" liner plugged with cement material (Figure 5).

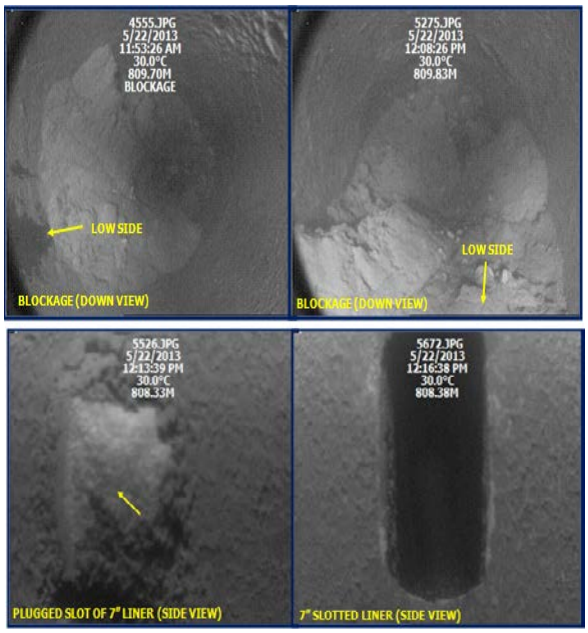

Figure 5: DHV images in well T4 showing blockages and plugged slots

2.2 Objectives and Case Studies

The current study presents several well tests of well T4 using pressure transient data collected from injection/fall-off tests. The aim of the present work is to develop numerical models that match the transient well test data. The sets of downhole data were divided into four cases:

Case 1: Post drilling
The data set in this case was gathered from the injectivity/fall-off test after the completion of drilling well T4 in February 1, 1997.

Case 2: After cement damage
The data set in this case was gathered from the injectivity/fall-off test after the cement invaded well T4 from well T7 production casing cementing.

Case 3: After mechanical clearing
The data set in this case was gathered from the injectivity/fall-off test after the mechanical clearing of well T4.

Case 4: Post acid stimulation
The data set in this case was gathered from the injectivity/fall-off test after acid stimulation of well T4.

The preliminary analysis of the sets of data is done using well test analysis and interpretation software. Three different numerical models were then developed for each test using: (a) a 3D model with a refined grid, (b) a radial model, and (c) a 3D model with a radial grid embedded into the injection block. For the radial-grid, three different models were further investigated: (a) homogeneous porous model, (b) fractured media model, and (c) a fractional dimension (fractal) model.

3. PRESSURE TRANSIENT ANALYSIS

SAPHIR™ transient well test analysis tool was used for the well test analysis of the well test data at different stages.

3.1 Post Drilling Completion Test

For case one, the well test analysis showed good matches with the measured data for the history plot (Figure 6), semi-log plot (Figure 7) and the log-log plot (Figure 8). The blue circle in Figure 6 shows the unstable pressures recorded during the late part of the fall-off test, which may be related to a two-phase effect. With the reduced flow rates of injected fluids during fall-off, high enthalpy fluids may be entering the feed zones causing these unstable pressures. The change in slope in the late part of the semi-log plot (Figure 7) showed a presence of a fault boundary. This was supported by a good fit of the unit slope line (Orange line) with the data in the log-log plot (Figure 8). The optimized reservoir parameters to the data set for case one: Post drilling is shown in Table 1. The model that gave the best match was of homogeneous reservoir and bounded by a fault estimated to be 109 meters away from the well. The permeability for this well is 16 mD. A negative value for skin indicates that the well has no wellbore damage.

Table 1. Optimized parameters for Case 1: Post drilling

Case 1: Post drilling	
Reservoir	Homogeneous
Boundary	One fault at 109 m
Initial Pressure	4883.8 kPa
Permeability (k)	16 mD
Skin (s)	-2.04
Thickness (h)	100 m

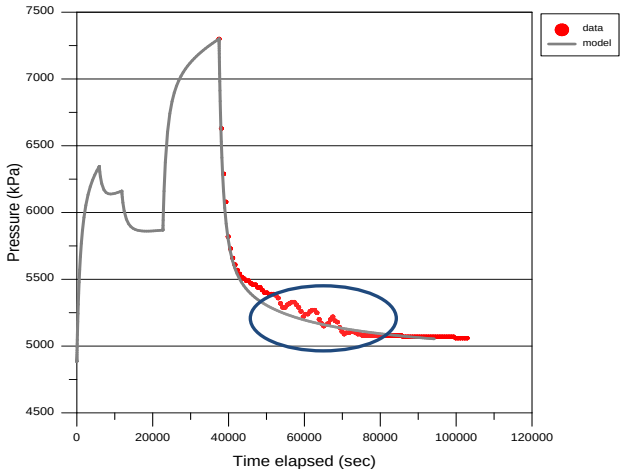

Figure 6: Post drilling history plot

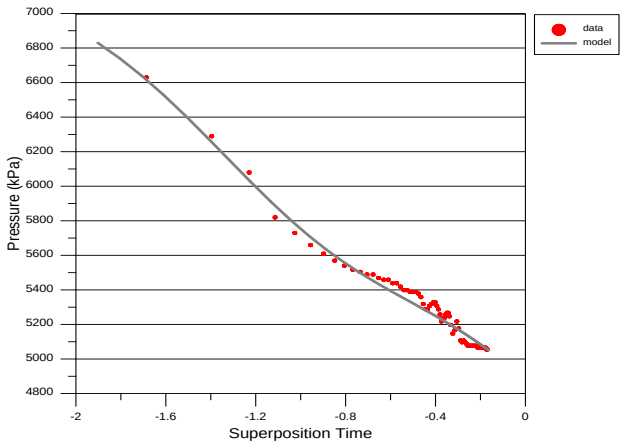

Figure 7: Post drilling semi-log plot

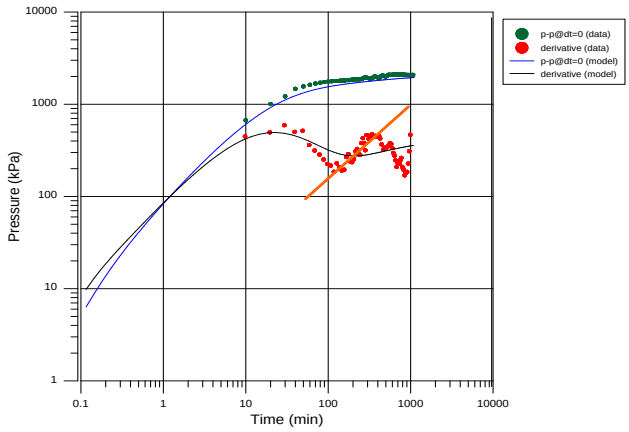

Figure 8: Post drilling log-log plot

3.2 After Cement Damaged

For case two, well test analysis gave reasonable matches with the measured data. Figures 9, 10 and 11 show the history plot, semi-log plot and log-log plot, respectively. The reservoir parameters for this case are summarized in Table 2. The best match was still achieved using a homogeneous reservoir model bounded by a fault. The fault is estimated to be 149 meters away and is supported by a good fit of a unit slope line (Orange line) with the data (Figure 11). The initial reservoir pressure decreased from 4883 kPa in case one to 1215 kPa in this case is attributable to the decline in reservoir pressure due to cement damage and also to production for 14 years. A positive skin is expected since cement clogged the near well bore zones of this well. The cement damage also resulted in a near wellbore low permeability value of 6.67 mD.

Table 2. Optimized parameters for Case 2: After cement damaged

Case 2: After cement damaged	
Reservoir	Homogeneous
Boundary	One fault at 149 m
Initial Pressure	1215.2 kPa
Permeability (k)	6.67 mD
Skin (s)	+14.9
Thickness (h)	100 m

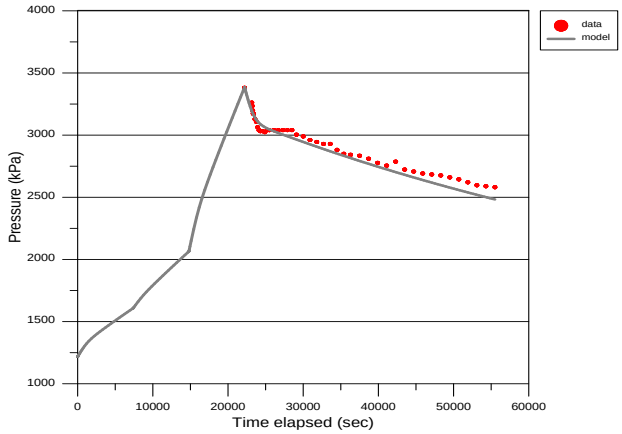

Figure 9: After cement damaged history plot

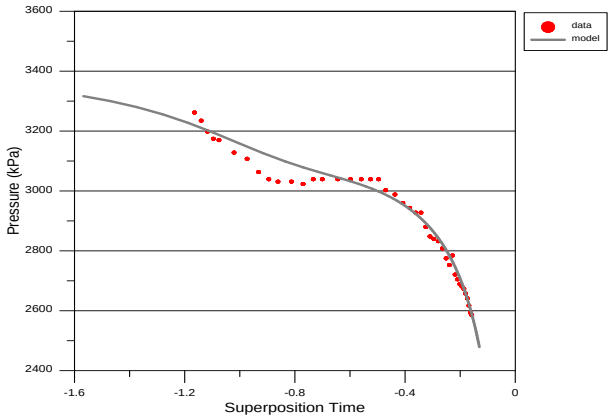

Figure 10: After cement damaged semi-log plot

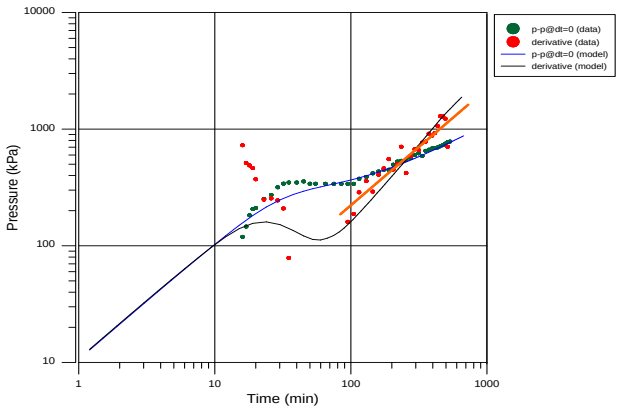

Figure 11: After cement damaged log-log plot

3.3 After Mechanical Clearing

For case three, well test analysis showed good matches with the measured data for the history plot (Figure 12), semi-log plot (Figure 13) and the log-log plot (Figure 14). Table 3 shows the optimized reservoir parameters. In this case, the best match is obtained from having a homogeneous reservoir and one fault boundary. The fault is estimated to be 165 meters away from the well. It can be observed that the initial pressure almost doubled after the well is mechanically cleared indicating contribution of feed zone. A negative value for skin indicates that the mechanical clearing done was effective for removing most of the wellbore damage.

Table 3. Optimized parameters for Case 3: After mechanical clearing

Case 3: After mechanical clearing	
Reservoir	Homogeneous
Boundary	One fault at 165 m
Initial Pressure	2256.4 kPa
Permeability (k)	201 mD
Skin (s)	-2.61
Thickness (h)	100 m

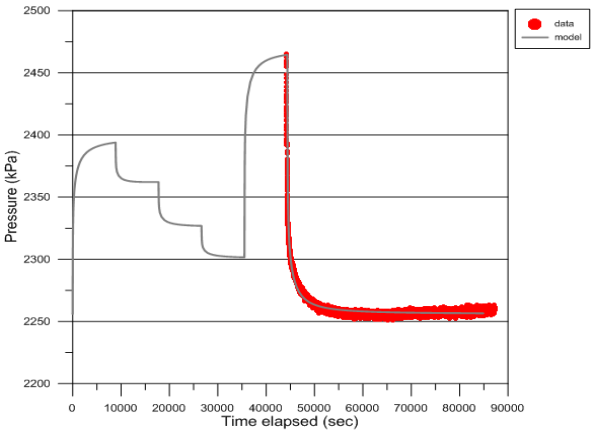

Figure 12: After mechanical clearing history plot

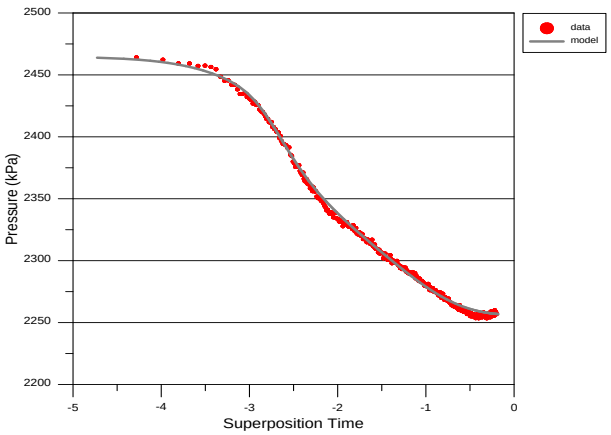

Figure 13: After mechanical clearing semi-log plot

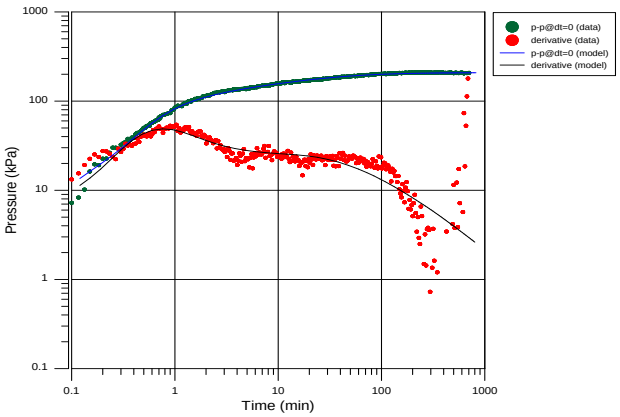

Figure 14: After mechanical clearing log-log plot

It can be observed that permeability increased to 201 mD in case three (After mechanical clearing) from 16 mD in case one (Post drilling). This permeability enhancement can also be attributable to production of 14 years. This is supported by the increase in injectivity index from 17.4 L/s-MPa in case one to 104.8 L/s-MPa in case three (Figure 15). Also, one notable point is the decline in reservoir pressure from 6-7 MPag in case one to 2-3 MPag in case three due to production.

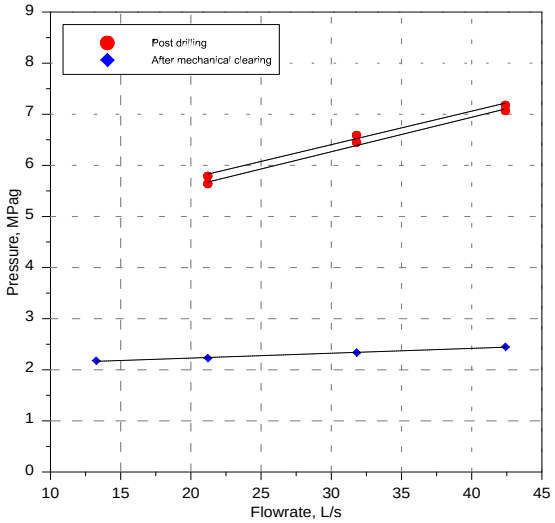

Figure 15: Well T4 injectivity plots for post drilling, after mechanical clearing and post acid stimulation

3.4 Post Acid Stimulation

In the last case, good matches were generated for the set of measured data. Figures 16, 17 and 18 show the history plot, semi-log plot and log-log plot, respectively. It has been consistent that a homogeneous reservoir model with fault boundary gave the best match. The fault is estimated to be 127 meters away from the well. It can be observed that the initial pressure increased from 2256.4 kPa to 2446.7 kPa when compared to case three. Permeability increased from 201 mD to 217 mD. Also, skin improved from -2.61 to -3.96. These all indicate that acid stimulation further enhanced the permeability of the well and dissolved the cement near the wellbore but mainly in the formations that cannot be accessed by mechanical clearing. The blue circle in Figure 16 shows the unstable pressures recorded during late part of the fall-off test. This was also experienced during post-drilling fall-off test (Figure 6) and may be related to a two-phase effect. With the reduced flow rates of injected fluids during fall-off, high enthalpy fluids may be entering the feed zones causing these unstable pressures.

Table 4. Optimized parameters for Case 4: Post acid stimulation

Case 4: Post acid stimulation	
Reservoir	Homogeneous
Boundary	One fault at 127 m
Initial Pressure	2446.7 kPa
Permeability (k)	217 mD
Skin (s)	-3.96
Thickness (h)	100 m

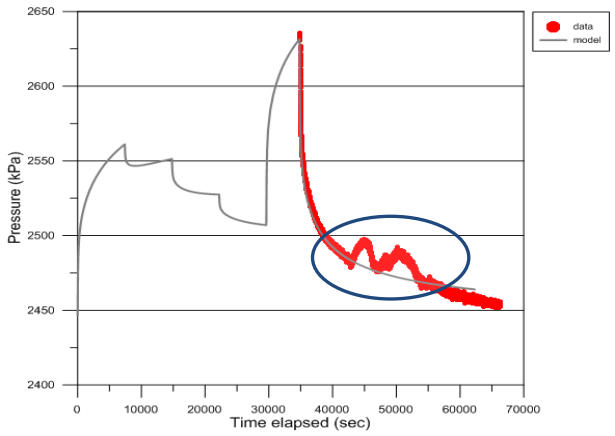

Figure 16: Post acid stimulation history plot

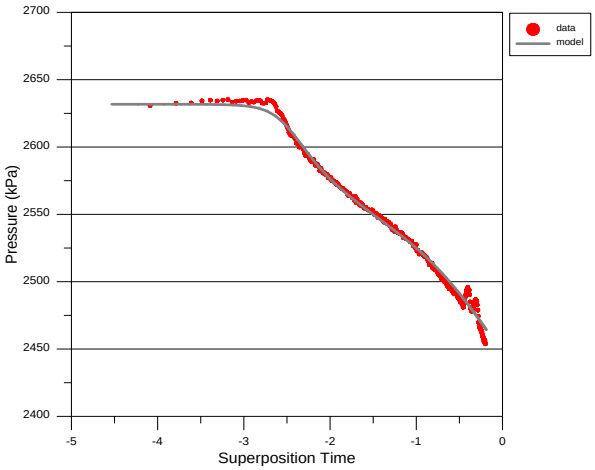

Figure 17: Post acid stimulation semi-log plot

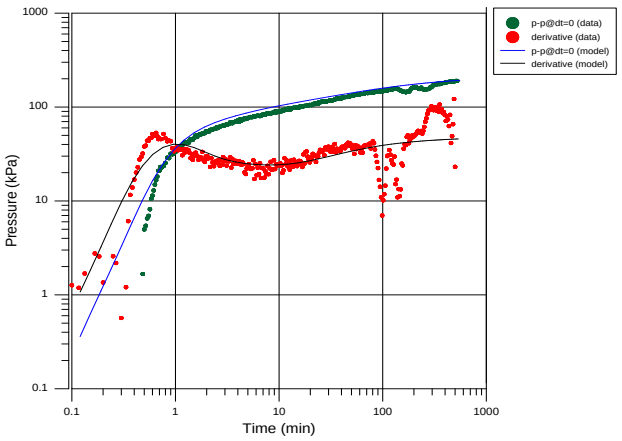

Figure 18: Post acid stimulation log-log plot

4. NUMERICAL MODELLING

4.1 3D numerical model with a refined grid

A large scale numerical model of the Mt. Apo geothermal field developed by Emoricha, et al. (2010) using the TOUGH2 simulator (Pruess, 1991; Pruess et al., 1999) was considered for matching the well test data. This model considers a total area of 572 km^2 (22 km by 26 km) encompassing the 701 hectares geothermal reservation (Figure 19). It was divided into 31 by 47 blocks and 19 layers giving a total of 27,683 blocks of which 16,411 are active elements in the model. Larger grid blocks cover the area outside the production sector. From a grid of 200m × 200m of the central block of interest on a full scale model, a small model was created with a smallest grid size of 12.5m × 12.5m. Figure 20 shows the refined grid of the small model. Top and bottom generators assigned to blocks located outside of the new grid were deleted. All the parameters (PARAM) inputs from the original input file were retained in the small model input file. The new natural state model input file was then generated and run in TOUGH2. The new model need not be recalibrated as the simulated data still matched the natural state data.

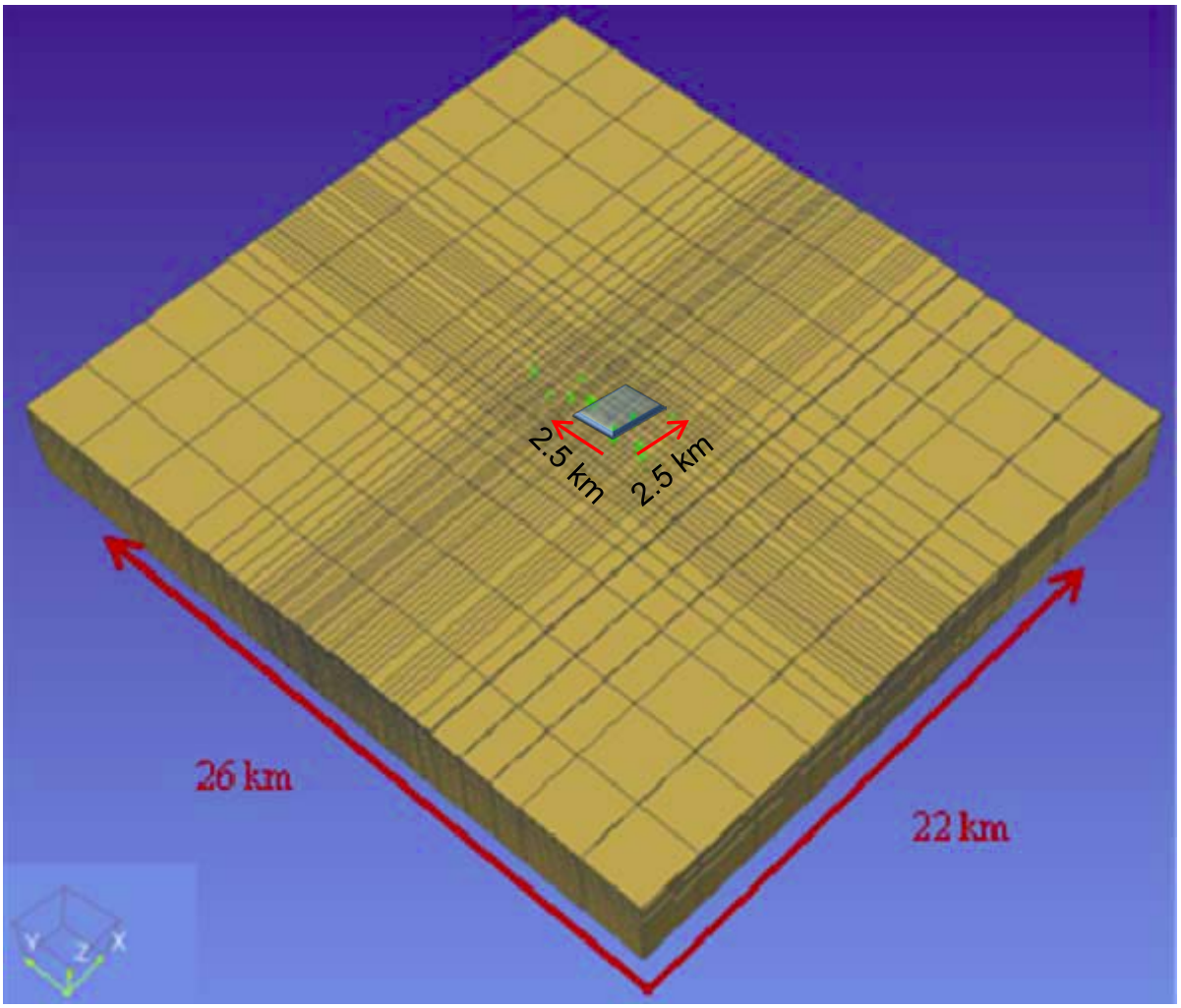

Figure 19: 3D grid block of the full scale model by Emoricha, E.B., et al. (2010) and the area of the small model shown in Figure 20.

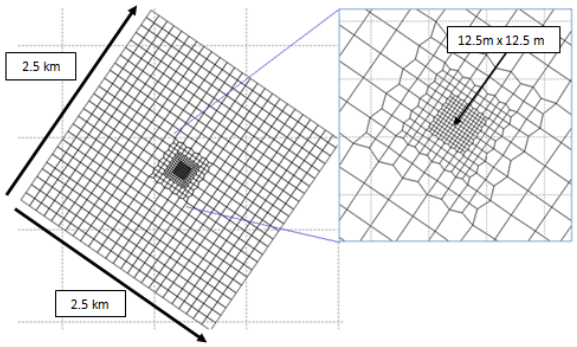

Figure 20: Grid of the small model

4.1.1 Results of the 3D model with a refined grid

The modeling results showed reasonable matches with the measured data for case one (Post drilling), case two (After cement damaged) and case three (After mechanical clearing) (Figures 21-23). However, the numerical model in all cases behaved like a fractured media where pressure changes abruptly with the change in flow rate. It can also be noted that the model generates higher pressures at higher injection rates than the measured data.

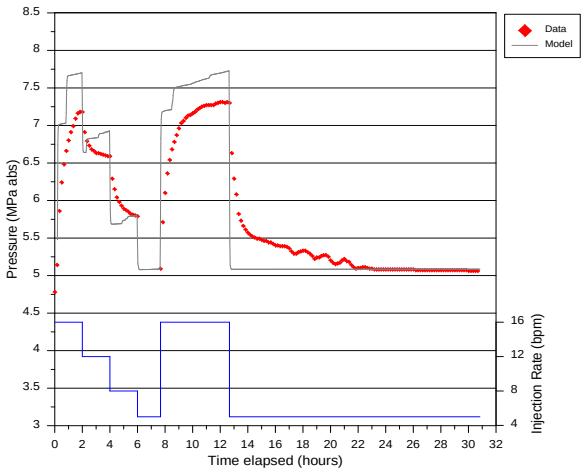

Figure 21: Post drilling modelling results using refined grid 3D model

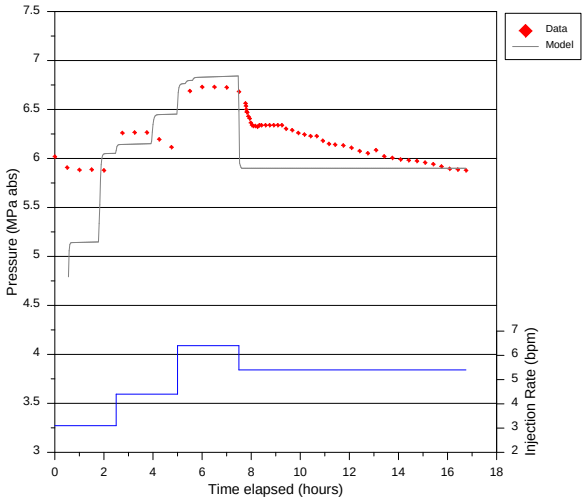

Figure 22: After cement damaged modelling results using refined grid 3D model

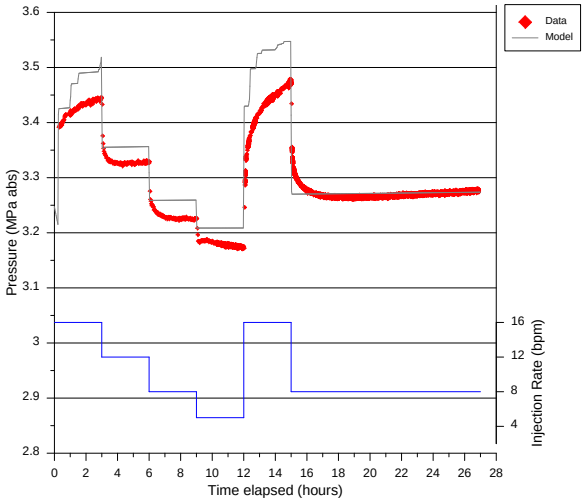

Figure 23: After mechanical clearing modelling results using refined grid 3D model

The match obtained in case four (Post acid stimulation) between the model and the data was relatively poor especially the part of the injectivity test where 5 bpm of fluid was injected (Figure 24). The black circle in the figure shows that instead of having lower pressures because of the decrease in injection rate from 8 bpm to 5 bpm, the pressure increased and became unstable. This may be related to two-phase well bore effects. With the reduced flow rates of injected fluids, high enthalpy fluids may be entering the feed zones causing these unstable pressures within the well. This is also experienced during the fall-off test illustrated by the blue circle.

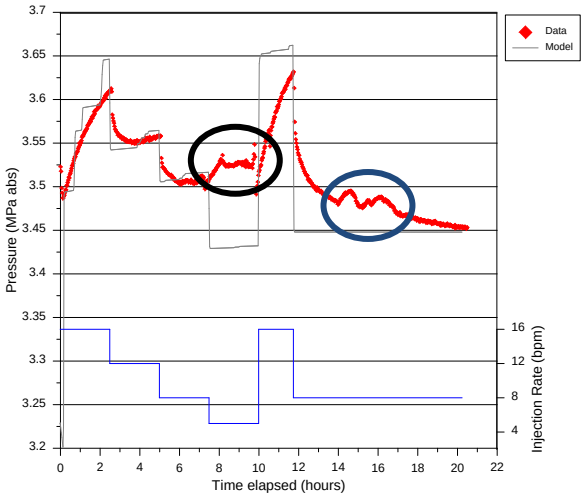

Figure 24: Post acid stimulation modelling results using refined grid 3D model

Figure 25 shows the pressure distribution during injection in case three (After mechanical clearing). From the injection block represented by block 1, pressure from injecting fluids is distributed to blocks 2-5, then again distributed to its adjacent blocks. It can be observed that using a rectangular grid, pressure cannot be distributed equally from the injection block to its surrounding blocks. In this case, pressure cannot be distributed directly from

injection block 1 to blocks 6-9 but through blocks 2-5. It is possible that using a nine point differencing scheme can help resolve this problem (McDowell et al, 2015).

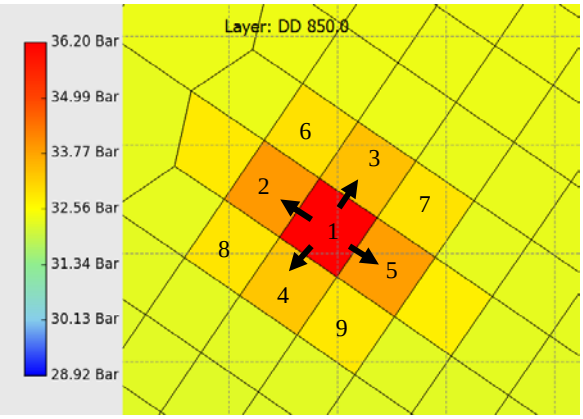

Figure 25: Pressure distribution during injection for case 3 (After mechanical clearing)

4.2 Radial flow models

In the radial flow numerical model, the reservoir is represented as a single layer and uses a radially symmetric mesh with the well located in the centre. The radial grid, shown in Figure 26, consists of 99 elements. The first element representing the well has a radius of 0.15 m and the width of the remaining elements increases by a constant factor of 1.1. The thickness of the layer is 100m.

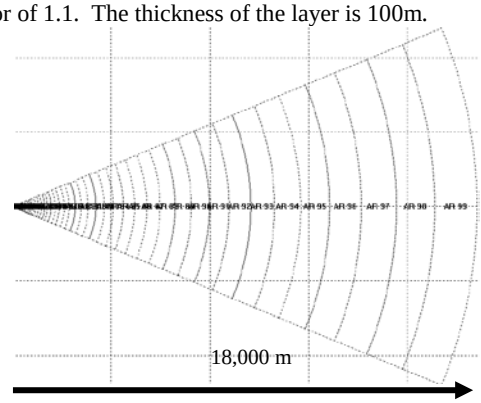

Figure 26: Radial grid

4.2.1 Homogeneous porous model

In this model it is assumed that the reservoir consists of a homogenous porous medium throughout. Skin effect was taken into consideration using different permeability blocks near the wellbore. As for the rest of the model blocks, similar permeability and porosity were assigned. Permeability was then varied to maximize agreement between model results and field data.

4.2.2 Fractured media model

When modeling fracture/matrix flow, a three layered model structure is used. Two layers for representing the rock matrix and a layer in between for representing the fracture. The number of elements per layer and the reservoir radius remained the same.

The fracture/matrix model assumed that the reservoir is not homogeneous, but made up of rock matrix blocks with high storativity and low permeability. The well is connected by natural fissures or fractures of low storativity and high permeability. The model was set up with one highly permeable fractured layer located between two matrix layers with lower values of permeability and porosity. Permeability was then varied in the fracture zone to maximize agreement between model results and field data.

4.2.3 Fractional dimension (fractal) model

In this model, the feed zone was made up of complex network of fractures. These are characterized by a non-integer dimension (n), having a geometric structure somewhere between two and three dimensions. The fractional dimension model represented the fractures by a continuum approach rather than by modelling them explicitly. This was done by modifying the specifications of block volumes and interface areas of the homogeneous porous layer model, according to the following equations:

$$V_i = \frac{\alpha_n b^{3-n}}{n} r_{i+1/2}^n - r_{i-1/2}^n \quad (1)$$

$$A_{i+1/2} = \alpha_n h^{3-n} r_{i+1/2}^{n-1} \quad (2)$$

$$\alpha_n = \frac{2\pi^{n/2}}{\Gamma(\frac{n}{2})} \quad (3)$$

where n is the dimension of the model, Γ is the Gamma function, Vi is the volume of the ith block located between radii r_i−1 and r_i, $A_{i+1/2}$ is the interface area located between the ith and (i + 1) blocks at a radius of $r_{i+1/2}$, and h is the layer thickness. Zarrouk, et al. (2007) showed that the optimized models had a dimension (n) close to 2.5. For this study, a value of n =2.5 for the dimensions used.

4.2.4 Results of the Radial flow models

In all cases, the best match to the measured data is given by the homogenous porous model (Figures 27-30). It can be observed in the plots that the homogenous porous model closely depicts the behavior of the measured data where there is a gradual change in pressure with changing injection flow rates.

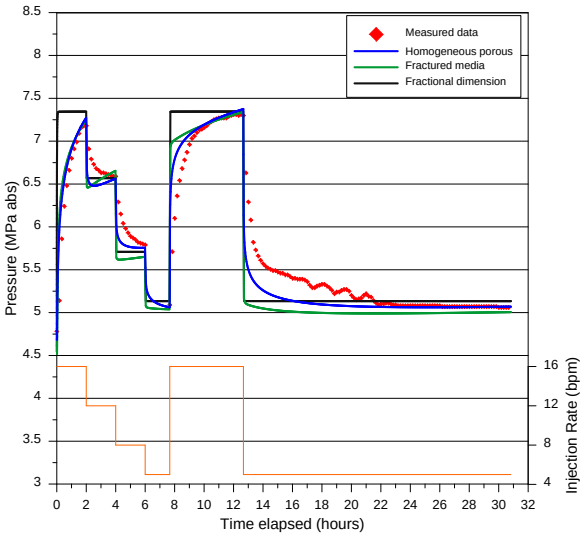

Figure 27: Post drilling modelling results using the different radial flow models

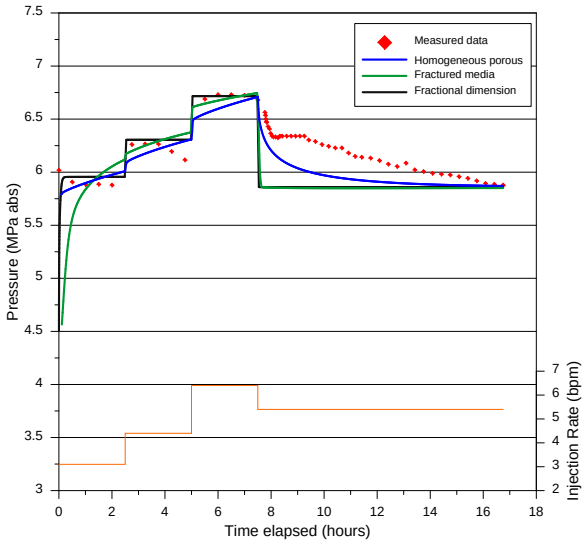

Figure 28: After cement damaged modelling results using the different radial flow models

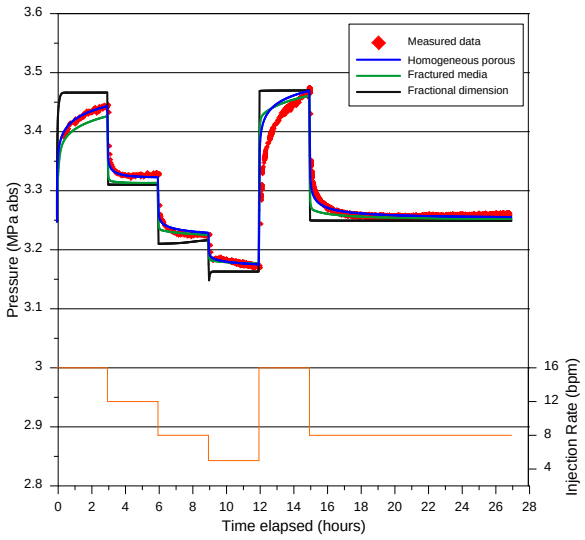

Figure 29: After mechanical clearing modelling results using the different radial flow models

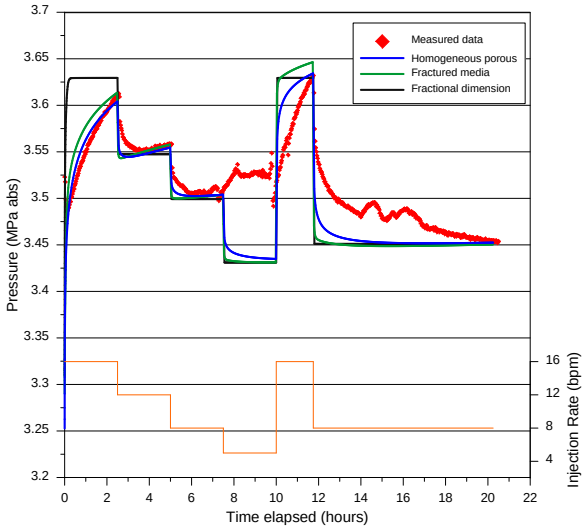

Figure 30: Post acid stimulation modelling results using the different radial flow models

4.3 3D Model with a radial grid embedded into the injection block

Within the model of Emoricha, et al. (2010), a radial grid from the homogenous porous model was embedded into the injection block. At the start, the total volume of the embedded radial blocks is about 25% of the original volume of the block. This was increased to 75% of the original volume of the block to determine any improvement on the matches. Embedded radial grids allow a more accurate representation of the near-wellbore behaviour while the larger blocks represent the field wide processes. The radial grid from the homogenous porous model was used since it had the best match from all the radial flow models.

4.3.1 Results of the embedded grid model

Reasonable matches were generated by the model in all cases with the embedded radial blocks of about 75% of the original volume of the block (Figure 31-34). There was no improvement observed on the match as the volume of the embedded radial blocks increased to 75% from 25%. This may also be attributable to the number of radial blocks embedded to the block. In the radial flow model, 99 radial blocks were used to have good matches. In this case, only 44 radial blocks were used to satisfy the 75% volume of the original block requirement. No further increase in volume of radial blocks embedded can be done for it will be more than the volume of the rectangular grid.

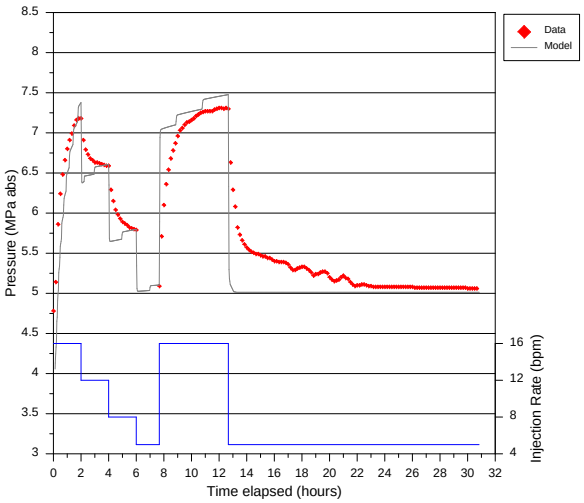

Figure 31: Post drilling modelling results using 75% volume

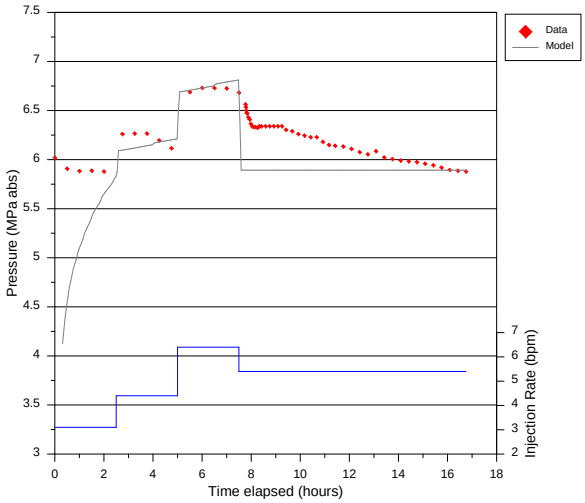

Figure 32: After cement damaged modelling results using 75% volume

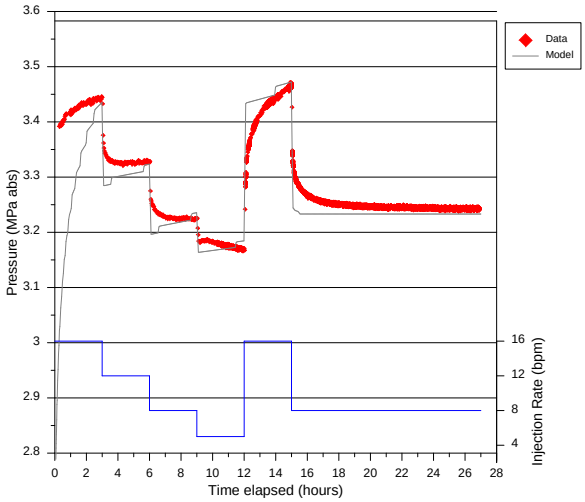

Figure 33: After mechanical clearing modelling results using 75% volume

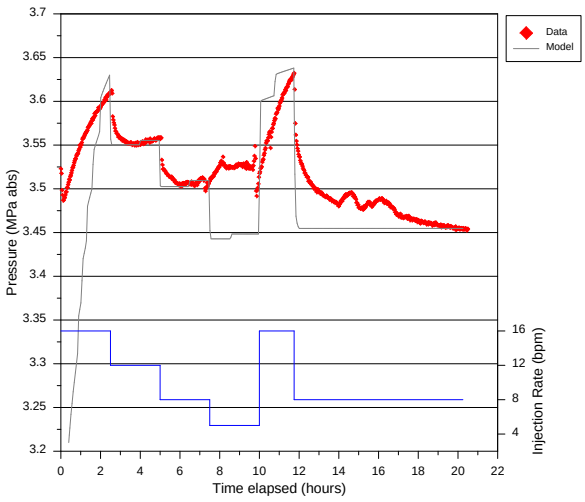

Figure 34: Post acid stimulation modelling results using 75% volume

The permeability for each case using pressure transient analysis, MDH (semi-log) and numerical modelling are summarized in Table 5. The values of permeability for each case using the three different methods are relatively close and reasonable.

Table 5. Permeability for each case using pressure transient analysis, MDH and numerical modelling

Case	Permeability using pressure transient analysis (mD)	Permeability using MDH (mD)	Permeability using numerical modelling (mD)
1: Post drilling	16.0	21.9	17.0
2: After cement-damaged	6.67	7.03	5.65
3: After mechanical clearing	201	203	270
4: Post acid stimulation	217	221	230

5. CONCLUSION

Pressure transient well test analysis clearly showed that there is presence of fault near production well T4, which is likely to be a boundary fault. However, the distance between the well and the fault varies from 109m to 165m, which is acceptable. The exact distance between the well and the fault should not be sought from transient well test analysis only.

Pressure transient well testing in high enthalpy and steam wells are carried out using two-rate pressure falloff test under water injection to prevent two phase conditions from taking place during the test. However, this may not always be possible when two-phase fluid starts to influence the pressure falloff as shown in Figures 6, 16, 24. A longer pumping duration for the initial pump rate would have collapsed further the two-phase fluid and diminished its influence during the falloff period. Note that the injection (injectivity) test is effectively a step down test rather than a step up rate test.

Although the cement damage had likely took place due to the communication through the fault or a fracture, the reservoir largely behaved as homogenous porous media.

The well test data showed that T4 permeability and injectivity increased with time due to production. Re-drilling (work over) was possibly sufficient to restore the permeability/productivity of the well. This indicated that the cement damage is localized and has not affected all the feed zones in T4.

The results of the modeling study showed that the single layer homogenous porous media model produced the best match to the pressure transient well test data.

ACKNOWLEDGEMENT

The authors would like to thank Energy Development Corporation, Philippines for sponsoring this study and for the kind permission to publish the results.

REFERENCES

Bondocoy, D. B., et al. (1994). *Mindanao 1 Geothermal Project, Resource Assessment Update.* PNOC-EDC Internal Report.

Clotworthy, A. W., & Hingoyon, C. S. (1995). Injectivity for Vapour Dominated Feed Zones. *17th NZ Geothermal Workshop,* New Zealand.

Cox, B. L., & Bodvarsson, G. S. (1985). Nonisothermal Injection Tests in Fractured Reservoirs. *10th Workshop on Geothermal Reservoir Engineering,* Stanford University, Stanford, California, USA.

Croucher, A. E. (2011). PyTOUGH: a Python scripting library for automating TOUGH2 simluations. *33rd NZ Geothermal Workshop,* New Zealand.

Emoricha, E. B., Omagbon, J. B., & Malate, R. C. M. (2010). Three Dimensional Numerical Modeling of Mindanao Geothermal Production Field, Philippines. *35th Workshop on Geothermal Reservoir Engineering,* Stanford University, Stanford, California, USA.

Esberto, M. B., Nogara, J. B., Daza, M. V., & Sarmiento, Z. F. (1998). Initial Respose to Exploitation of the Mt. Apo Geothermal Reservoir, Cotabato, Philippines. *23th Workshop on Geothermal Reservoir Engineering,* Stanford University, Stanford, California, USA.

Houze, O., Viturat, D., & Fjaere, O. S. (2008). *Dynamic Flow Analysis.* KAPPA.

McDowell A., Zarrouk, S.J., and Clarke, R. (2015) Modelling Viscous Fingering During Reinjection in Geothermal Reservoirs. Proceedings World Geothermal Congress 2015, Melbourne, Australia, 19-25 April 2015.

Marasigan, R. (2014). *Mt. Apo Geothermal Project Map* EDC.

O'Sullivan, M. J., Croucher, A. E., Anderson, E. B., Kikuchi, T., & Nakagome, O. (2005). An Automated Well-test Analysis System (AWTAS). *Geothermics,* (34), 3-25.

Pastoriza, L. R., Austria, J. M. V., Batolbatol, J. R., Panem, C. C., & Reyes, J. K. (2013). *Unraveling the Philippines' Hightest: Geology of Mt. Apo, Kidapawan, North Cotabato, Philippines.* EDC Internal Report.

Pioquinto, W. C. (1997). *Geology of Well TM-4D.* PNOC-EDC Internal Report.

Pressure Transient Analysis. (2014). Retrieved June 2, 2014, Retrieved from http://www.kappaeng.com/software/saphir

Pruess, K., Oldenburg, C. and Maridis, G. (1999). TOUGH2 USER'S GUIDE, VERSION 2.0. Earth Sciences Division, Lawrence Berkeley National Laboratory, University of California, Berkeley, California 94720. LBNL-43134.

Pruess, K., & Enedy, S. (1993). Numerical Modeling of Injection Experiments at the Geysers. *18th Workshop on Geothermal Reservoir Engineering,* Stanford University, Stanford, California, USA.

Pruess, K. (1991). *TOUGH2: A general-purpose numerical simulator for multiphase fluid and heat flow.* Lawrence Berkeley National Laboratory, Berkeley, California, USA:

Puno, P., Newson, J., & Zarrouk, S. (2012). *Development of a Detailed Small Scale Numerical Model using PyTOUGH.* University of Auckland, Auckland, New Zealand:

Satman, A., Sarak, H., Onur, M., & Korkmaz, E. D. (2005). Modeling of Production/Reinjection Behavior of the Kizildere Geothermal Field by a Two-Layer Geothermal Reservoir Lumped-Parameter Model. *World Geothermal Congress 2005,* Antalya, Turkey.

Zarrouk, S.J., O'Sullivan, M., Croucher, A., & Mannington, W. (2007). Numerical Modelling of Production from the Poihipi Dry Steam Zone: Wairakei Geothermal System, New Zealand. *Geothermics,* (36), 289-303.